Supporting information

Tailoring the Pore Structure of Iron Oxide Core@Stellate Mesoporous Silica Shell Nanocomposites: Effects on MRI and Magnetic Hyperthermia Properties and Applicability to Anti-Cancer Therapies

Joëlle Bizeau[1], Justine Journaux-Duclos[2], Céline Kiefer[1], Barbara Freis[1], Dris Ihiawakrim[1], Maria de los Angeles Ramirez[1], Théo Lucante[1], Ksenia Parkhomenko[3], Charlotte Vichery[4], Julian Carrey[5], Olivier Sandre[6], Caroline Bertagnolli[7], Ovidiu Ersen[1], Sylvie Bégin-Colin[1], Véronique Gigoux[2], Damien Mertz*[1]

[1] Institut de Physique et Chimie des Matériaux de Strasbourg (IPCMS), UMR-7504 CNRS-Université de Strasbourg, 23 rue du Lœss, BP 34 67034, Strasbourg Cedex 2, France.

[2] Centre de Recherches en Cancérologie de Toulouse UMR1037 CNRS - Inserm/Université Paul Sabatier, 1 avenue Jean Poulhes, BP 84225, 31432 Toulouse, Cedex 4, France.

[3] Institut de Chimie des Procédés pour l'Energie, l'Environnement et la Santé (ICPEES), UMR-7515 CNRS-Université de Strasbourg, 25 rue Becquerel, 67087 Strasbourg, France

[4] Université Clermont Auvergne, Clermont Auvergne INP, CNRS, ICCF, F-63000 Clermont-Ferrand, France

[5] LPCNO (Laboratoire de Physique et Chimie des Nano-Objets), Université de Toulouse, CNRS, INSA, UPS, 31077 Toulouse, France

[6] Laboratoire de Chimie des Polymères Organiques (LCPO) UMR 5629 Univ. Bordeaux / CNRS / Bordeaux INP, 16 Avenue Pey-Berland, 33607 Pessac France

[7] Institut Pluridisciplinaire Hubert Curien (IPHC), UMR 7178 CNRS-Université de Strasbourg, 25 Rue Becquerel, 67087 Strasbourg, France

*Correspondance : damien.mertz@ipcms.unistra.fr

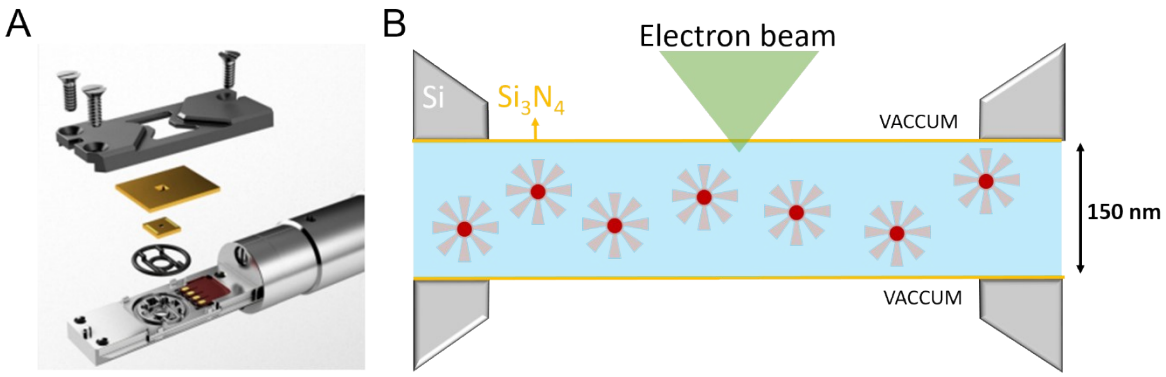

Figure S1: A) Scheme of the TEM holder with the specific LPTEM chips (Protochips website: www.protochips.com) B) Schematic representation of the bottom chip.

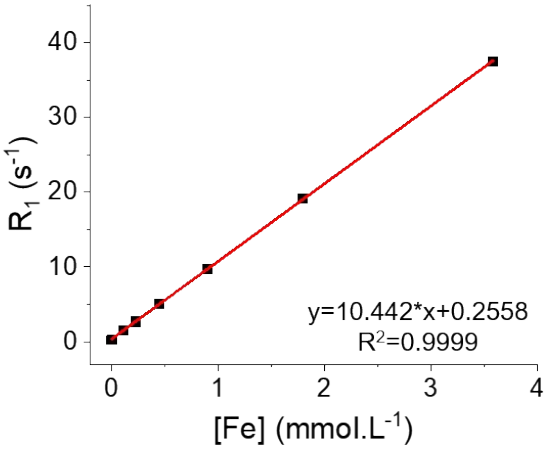

Figure S2: Calibration curve used for the iron titration by NMR ^{1}H-relaxometry.

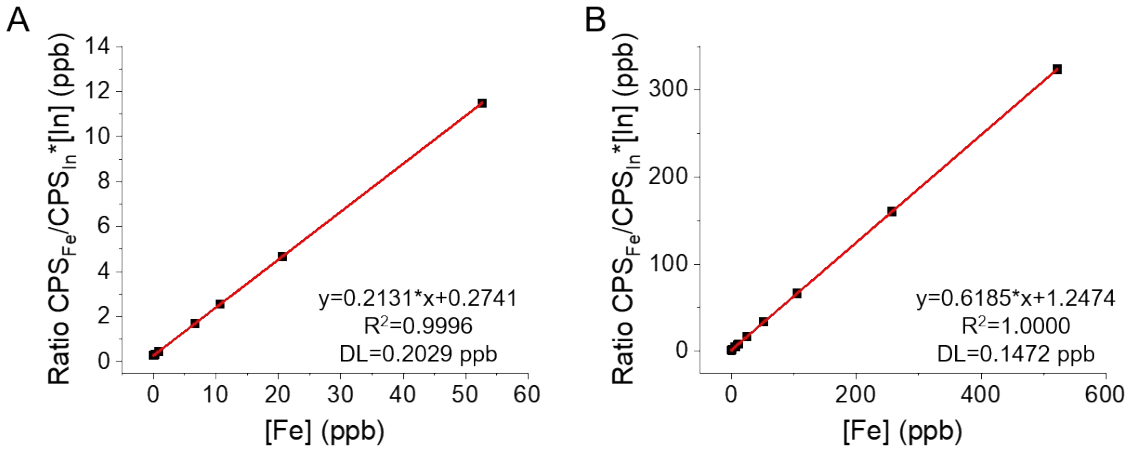

Figure S3: Calibration curves used for the iron titration by ICP-MS and for the biological samples incubated with A) 0.5 µgFe.mL^{-1} and B) 5 µgFe.mL^{-1}.

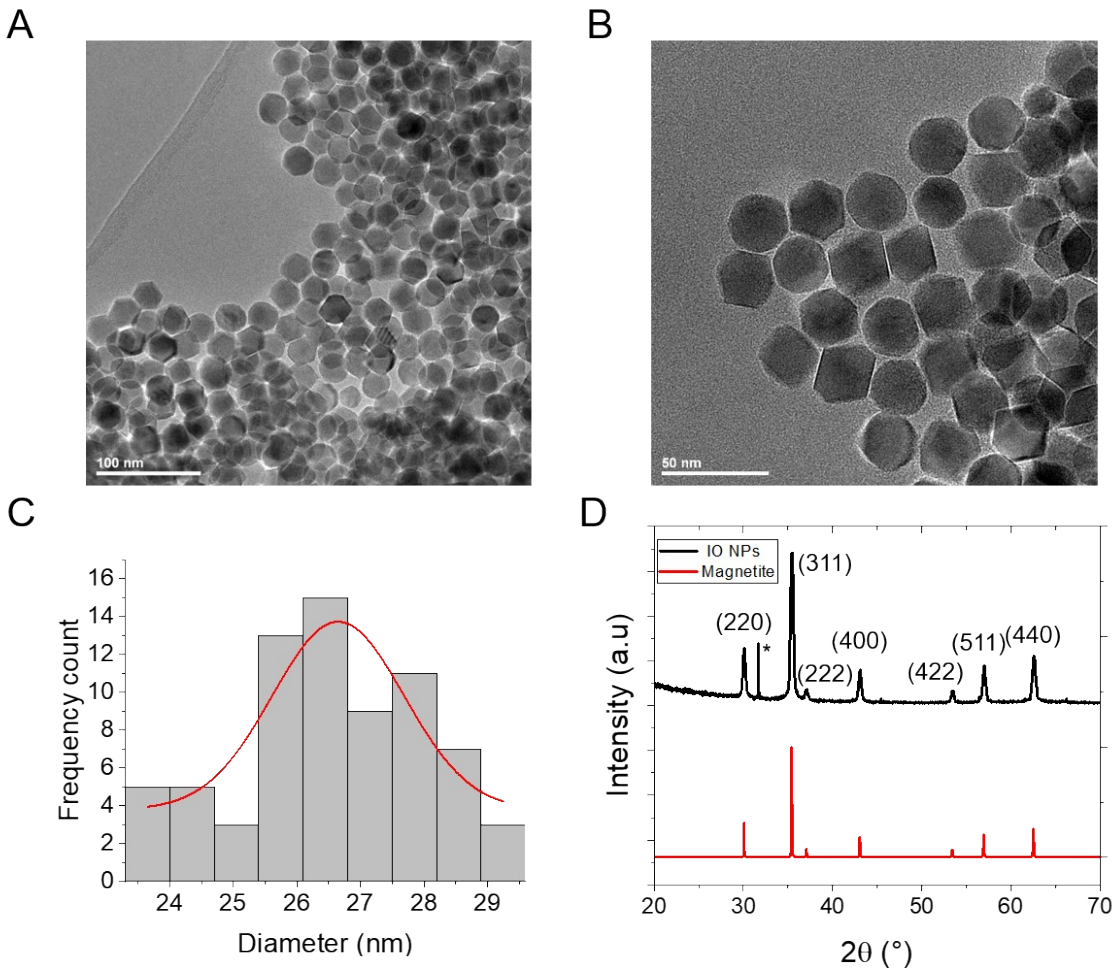

Figure S4: A) and B) TEM images of the IO NPs, C) Diameter distribution of the IO NPs with the Gaussian fit and D) XRD diffractogram of the IO NPs.

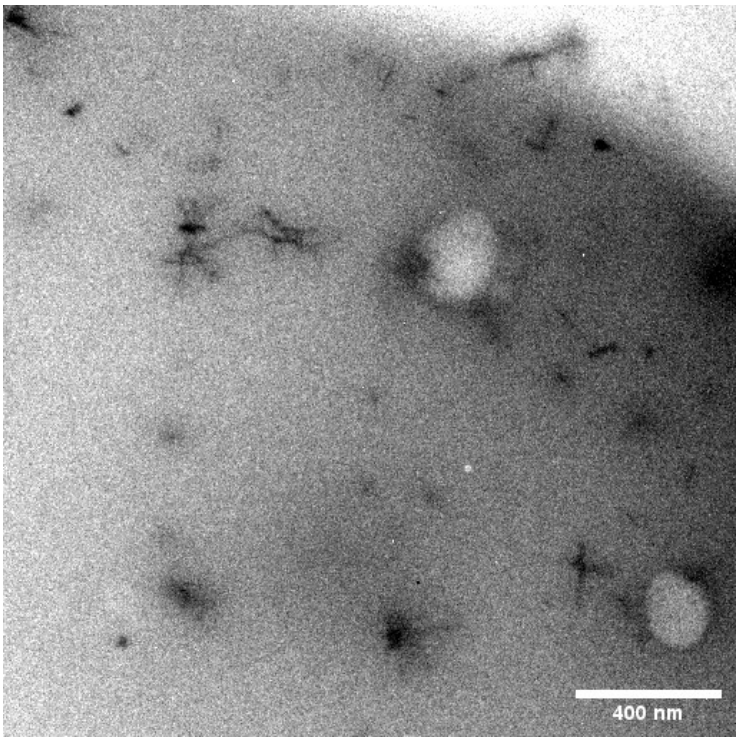

Figure S5: TEM image of another region of the chip used in the first *in situ* LPTEM experiment.

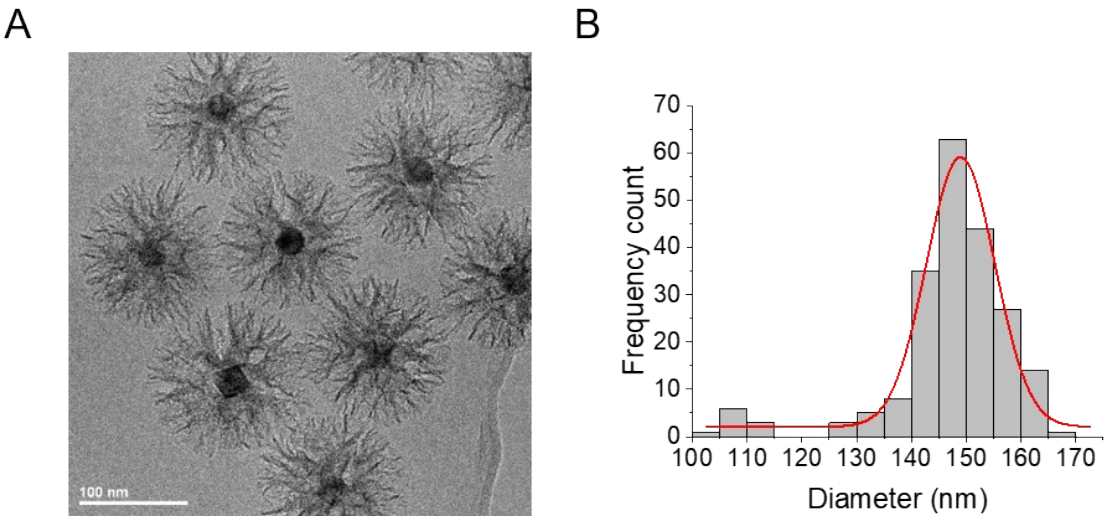

Figure S6: Characterization of the IO@STMS-90 A) TEM image. B) Diameter distribution analyzed with a Gaussian fit. Diameter 149±12 nm, 61.2 nm of SiO_2.

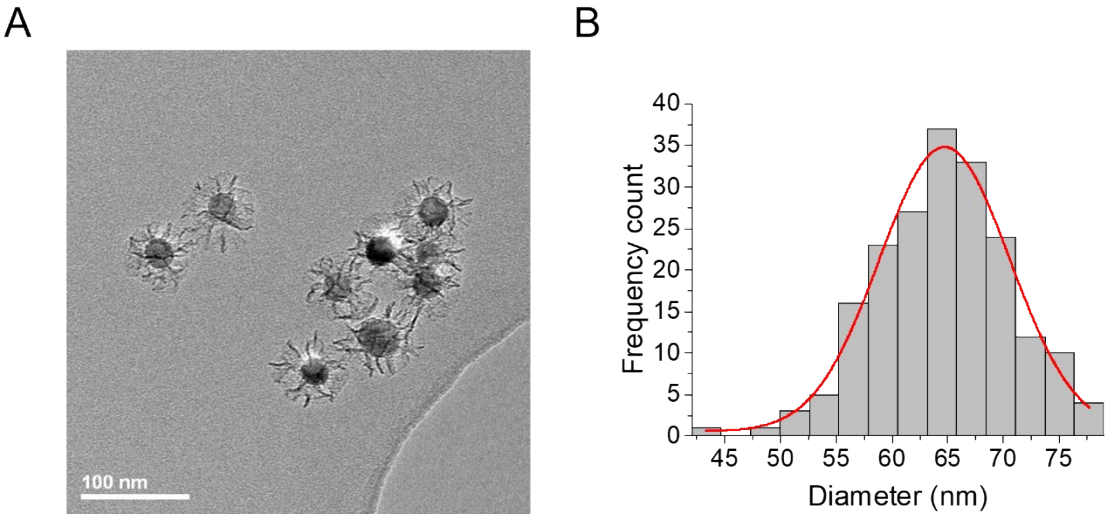

Figure S7: Characterization of the IO@STMS-40 obtained from a new batch of IO NPs (diameter 27.0±4.0 nm) A) TEM image. B) Diameter distribution analyzed with a Gaussian fit. Diameter 65±12 nm, 19 nm of SiO_2.

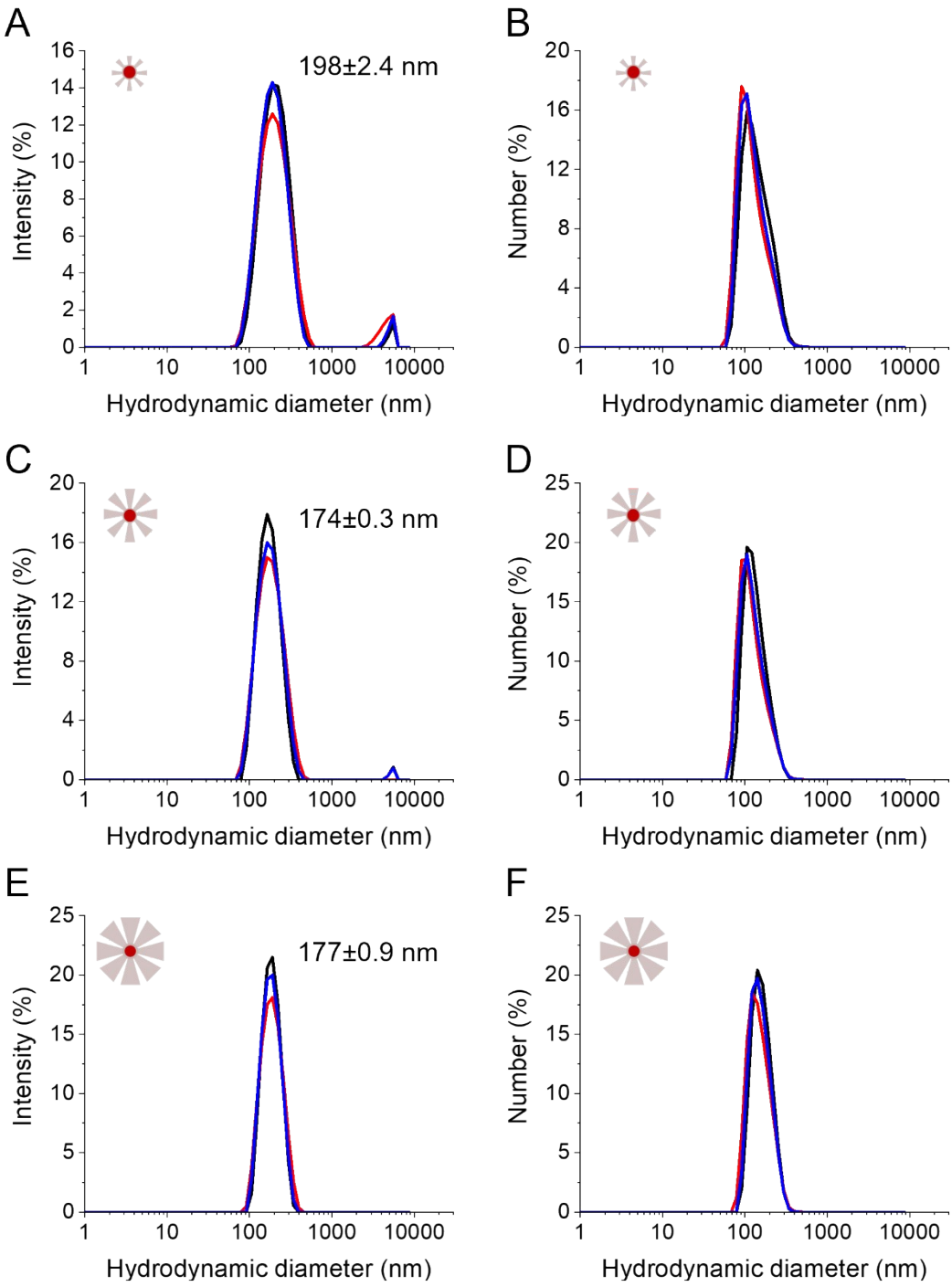

Figure S8: Colloidal stability in EtOH in intensity and in number respectively of IO@STMS-40 (A, B), IO@STMS-60 (C, D) and IO@STMS-120 (E, F).

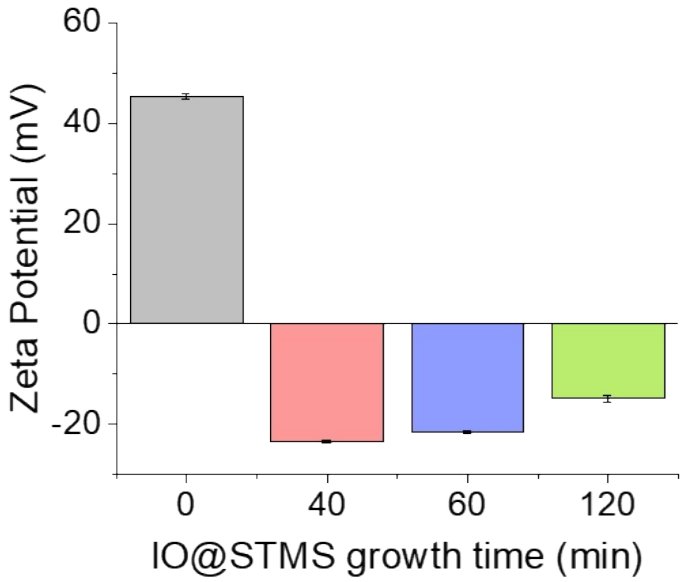

Figure S9: Zeta potential of the IO@STMS-t NPs in dH_2O.

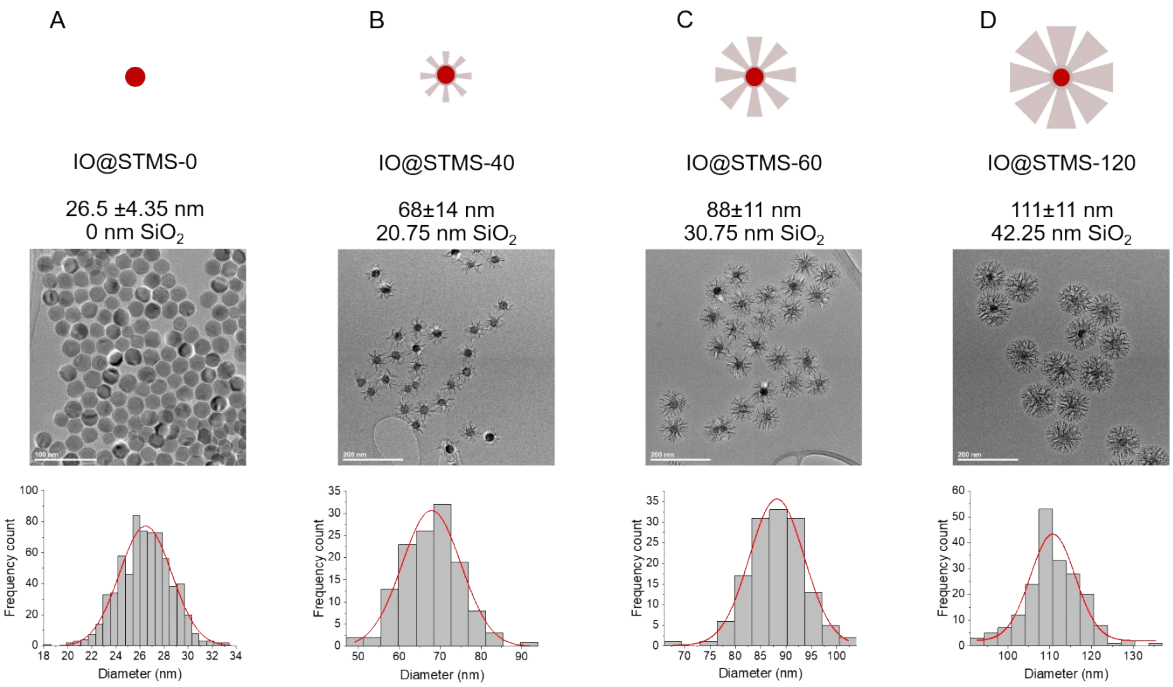

Figure S10: Schematic representation, TEM and diameter distribution of A) IO@STMS-0, B) IO@STMS-40, C) IO@STMS-60 and D) IO@STMS-120 obtained from series 2.

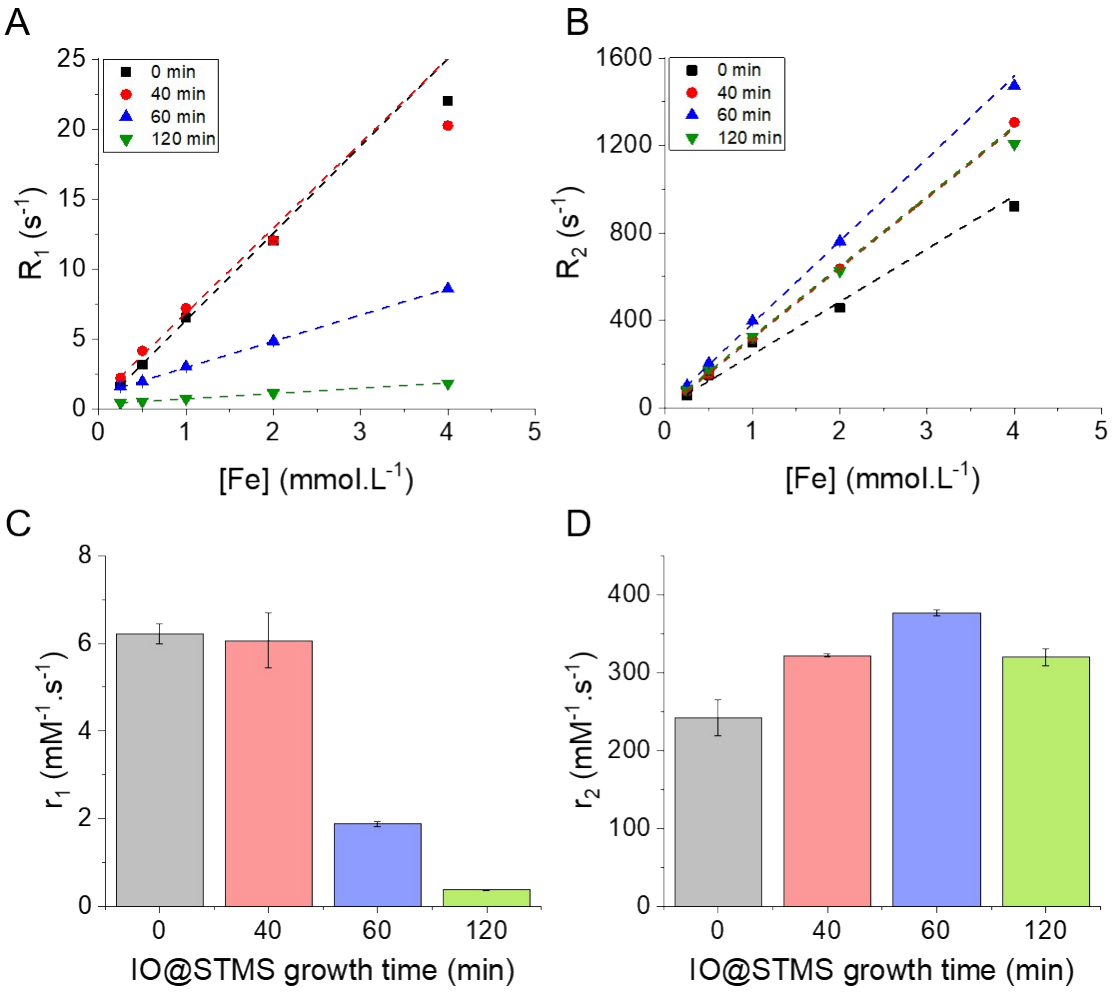

Figure S11: A) and B) respectively the longitudinal $R_1=1/T_1$ (s^{-1}) and transverse $R_2=1/T_2$ (s^{-1}) relaxation rates as a function of the concentration in iron in the different IO@STMS-t NPs solutions. C) and D) respectively the evolution of the longitudinal and transverse relaxivities r_1 and r_2 as a function of the IO@STMS growth time. These results were obtained with the IO@STMS-t obtained from series 1.

Table S1: Longitudinal (r_1) and transversal (r_2) numerical values measured for the IO@STMS-t NPs obtained from series 1.

Sample	r_1 ($mM^{-1}.s^{-1}$)	r_2 ($mM^{-1}.s^{-1}$)
IO@STMS-0	6.22±0.22	242±23
IO@STMS-40	6.06±0.63	322±2
IO@STMS-60	1.88±0.06	377±4
IO@STMS-120	0.38±0.01	320±11

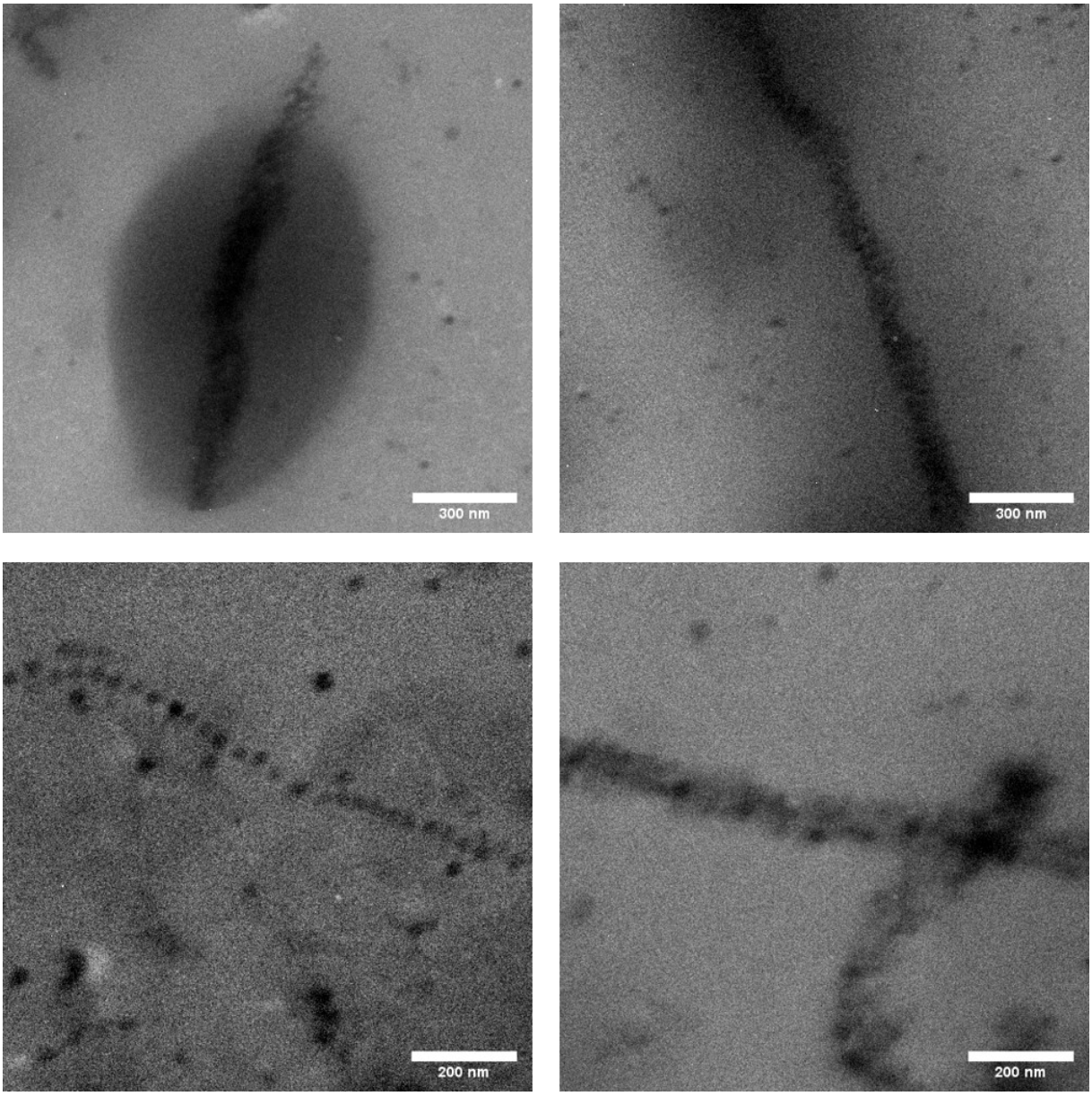

Figure S12: TEM images of IO NPs chain observed when performing the second *in situ* LPTEM experiment.

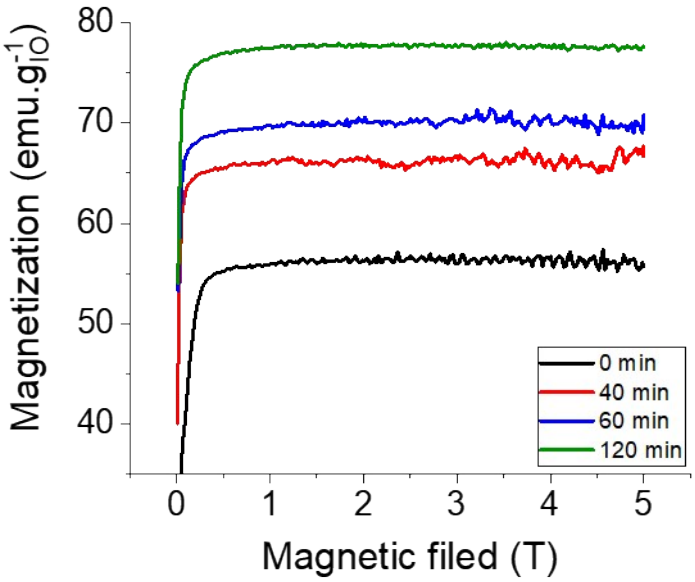

Figure S13: M(H) Magnetization curves of IO@STMS-t NPs at 300 K.

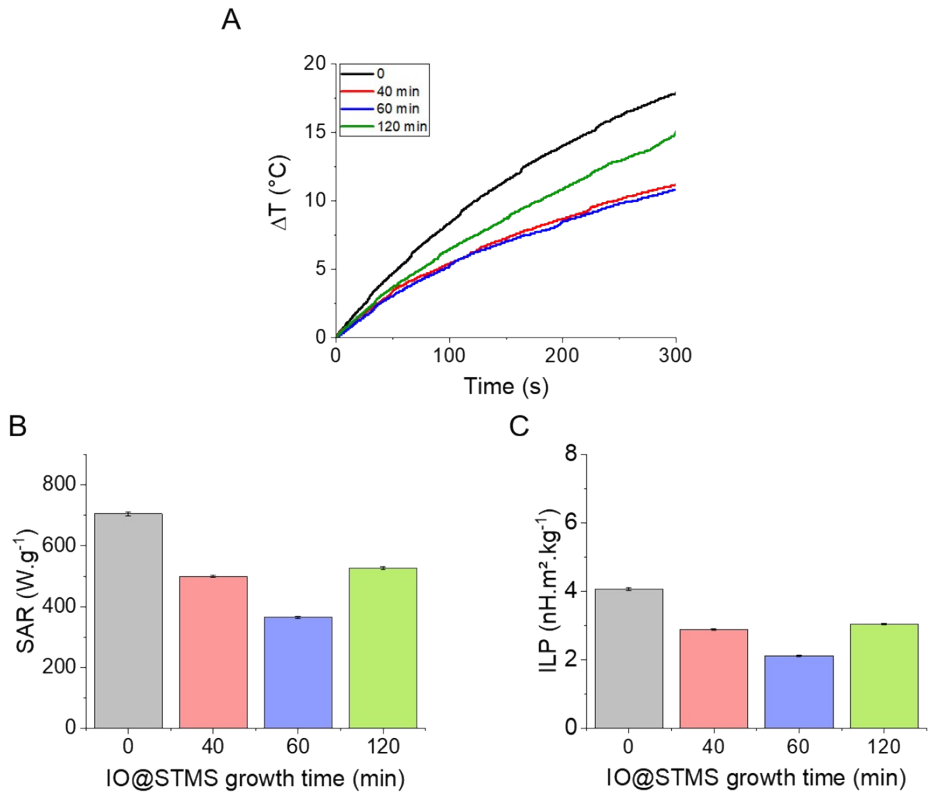

Figure S14: A) Temperature profiles as a function of time for the different IO@STMS-t NPs obtained from series 1 at 0.5 mgFe.mL^{-1} under AMF (303 kHz / 24 kA m^{-1}). B) Corresponding SAR values. C). Corresponding ILP values. Errors bars are coming from the fit.

The heating efficiency of IO@STMS-t NPs was first evaluated on the particles obtained from series 1 by calorimetry, but the diverse apparatus available in our lab or in our collaborators' labs went out of order while we needed to perform such analysis on the particles obtained from series 2, which explains the two techniques used for the two series of batches.

Table S2: SAR and ILP numerical values measured for the IO@STMS-t NPs obtained from series 1.

Sample	SAR (W.g^{-1})	ILP (nH.m^2.kg^{-1})
IO@STMS-0	705±7	4.08±0.04
IO@STMS-40	500±4	2.89±0.02
IO@STMS-60	365±4	2.11±0.02
IO@STMS-120	527±4	3.05±0.02

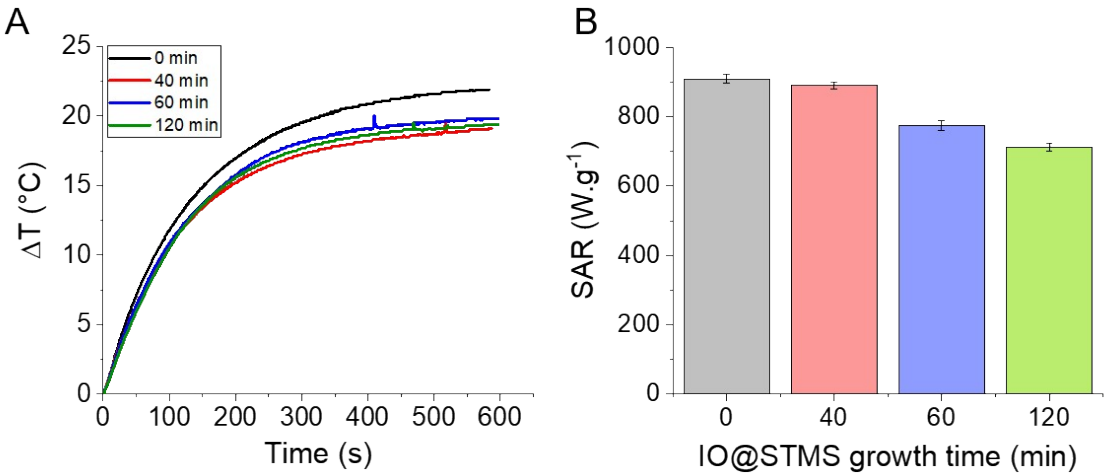

Figure S15: A) Temperature profiles as a function of time for the different IO@STMS-t NPs at 0.5 mgFe.mL^{-1} under NIR light irradiation. B) Corresponding SAR values. These results were obtained with the IO@STMS-t obtained from series 1. Errors bars are coming from the fit.

Table S3: SAR numerical values measured for the IO@STMS-t NPs obtained from series 1.

Sample	SAR (W.g^{-1})
IO@STMS-0	909±13
IO@STMS-40	891±10
IO@STMS-60	776±14
IO@STMS-120	712±12

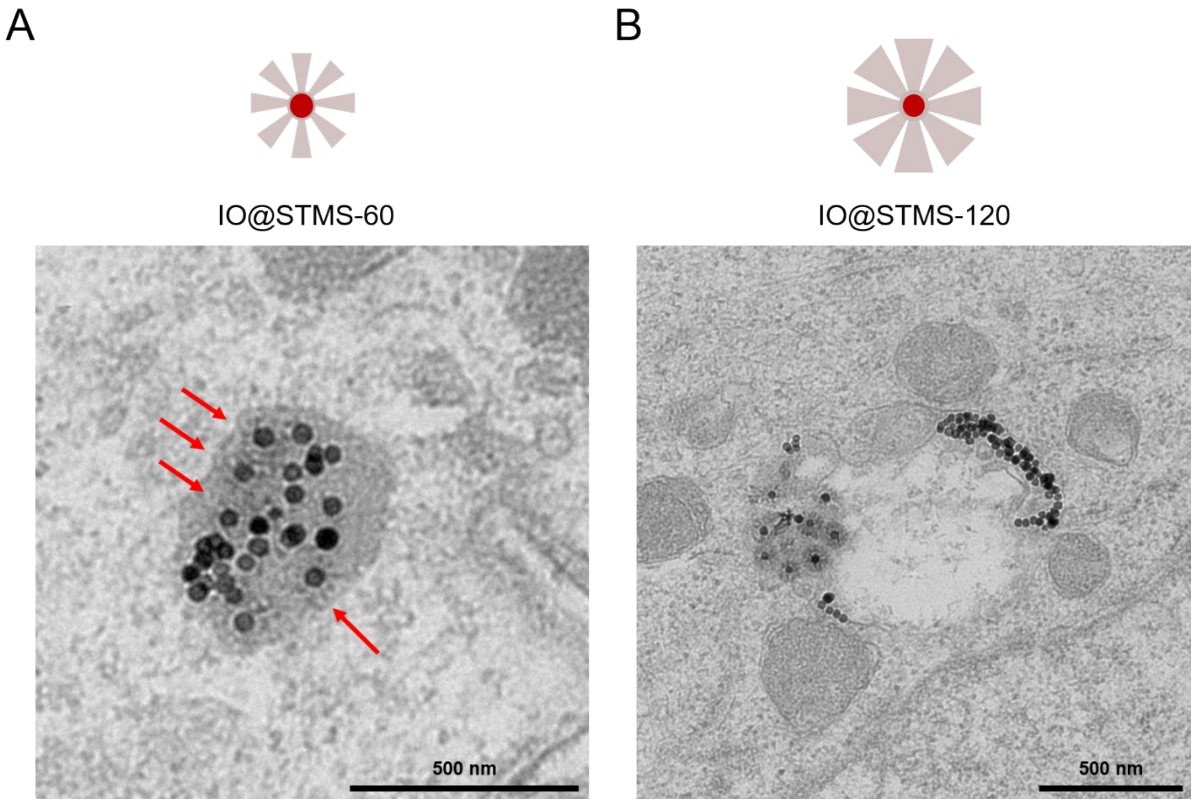

Figure S16: TEM images of cells incubated at 5 µgFe.mL^{-1} for 72 h with A) IO@STMS-60 and B) IO@STMS-120 where silica shell can still be observed.

Links to supplementary video files:

Please find below the two links of the videos hosted on the youtube channel of our institute (Youtube of IPCMS
Strasbourg) (https://www.youtube.com/channel/UC8liXtlkk2iEXT0AuVodPRQ)

Video 1 : https://youtu.be/Ea1hb5D4joU?si=iWRf_4QjIX_vgkMA

Video 2 : https://youtu.be/vtibyxpVuyU?si=0Lchm7C4AM7jxfCJ